ISSN 1615-9306 · JSSCCJ 48 (9) 2025 · Vol. 48 · No. 9 · September 2025

Journal of SEPARATION SCIENCE

9|2025

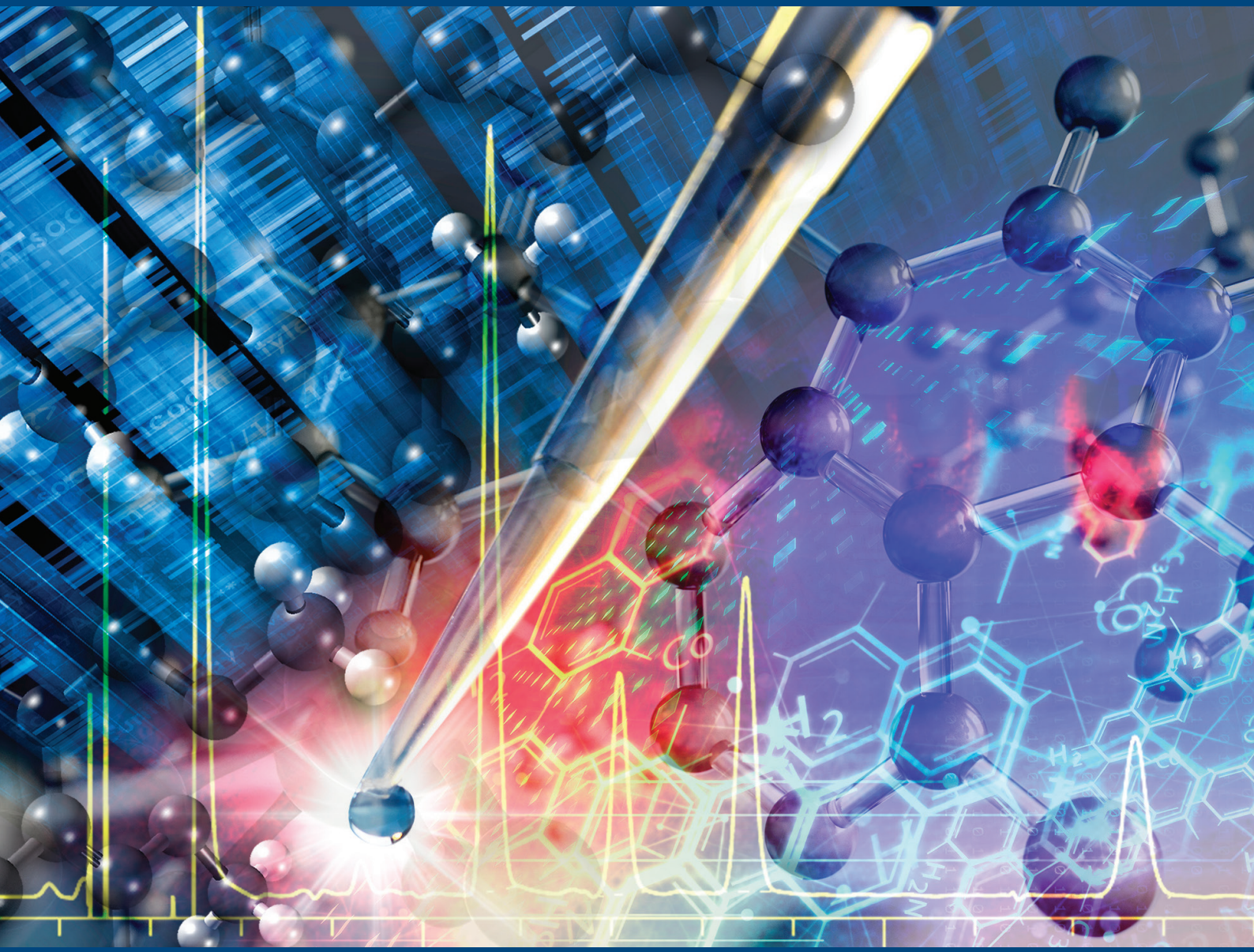

www.jss-journal.com

Methods
Chromatography · Electroseparation

Applications
Biomedicine · Foods · Environment

WILEY VCH

Journal of Separation Science

WILEY-VCH

JOURNAL OF SEPARATION SCIENCE

ORIGINAL ARTICLE

Metabolite Profiling of Guipi Pill Using UHPLC-Q-Orbitrap-HRMS and Determination of the Pharmacokinetics of its Major Prototype Components

Huafang Bai[1,2] | Hongjin Wang[1] | Nannan Yuan[1] | Hui Zhang[3] | Qi Sun[1] | Mengru Wang[3] | Jinwei Gao[3]

[1]School of Pharmacy, Shenyang Pharmaceutical University, Shenyang, China | [2]Yunnan Center for Animal Disease Control and Prevention, Kunming, China | [3]School of Pharmacy, Shenyang Medical College, Shenyang, China

Correspondence: Jinwei Gao (gaojinwei0903@163.com)

Received: 27 June 2025 | **Revised:** 14 August 2025 | **Accepted:** 18 August 2025

Funding: This work was supported by a rolling funding project for Liaoning distinguished professors (2017), and the Science Research Fund Project of Liaoning Provincial Department of Education (Grant Number. JYTMS20231404).

Keywords: Guipi Pill | in vivo | metabolism | pharmacokinetics | traditional Chinese medicine

ABSTRACT

Guipi Pill (GPP), a classic traditional formula used to treat anxiety disorders, demonstrates significant pharmacological activity. However, research on its pharmacodynamic material basis remains limited. UHPLC-Q-Orbitrap-HRMS was used to systematically analyze the metabolites of GPP in the blood, urine, bile, and feces of rats after oral administration and elucidate its in vivo metabolic processes. The pharmacokinetic characteristics of the major prototype components were determined using UHPLC-MS/MS. A total of 106 compounds (48 prototype components and 58 metabolites) were identified in GPP, which included the following six structural classes: phenylpropanoids, flavonoids and their glycosides, terpenoids and their glycosides, volatile oils, organic acids, and acetylenic glycosides. Nine of the metabolites were presumed to be novel compounds, which were previously unreported. Metabolic pathways involved Phase I reactions (hydrolysis, methylation, oxidation) and Phase II reactions (glucuronidation or sulfation of Phase I metabolites). Pharmacokinetic analysis revealed flavonoid glycosides (e.g., liquiritin) to exhibit a short time to attain maximum concentration (T_{max}), short elimination half-life ($t_{1/2}$), and short mean residence time (MRT), consistent with their structural features, whereas terpenoids (e.g., costunolide, atractylenolide I, dehydrocostus lactone, glycyrrhetinic acid) showed slow absorption, slow elimination, and a long MRT. The volatile oil, ligustilide, demonstrated rapid absorption and a long $t_{1/2}$. This study systematically delineates the metabolic characteristics and pharmacokinetic profiles of the major constituents of GPP in rats, providing a scientific basis for the further elucidation of its pharmacodynamic material basis and mechanisms of metabolic regulation.

1 | Introduction

Anxiety disorders represent a growing global health burden, with traditional Chinese medicine (TCM) formulations offering distinctive therapeutic advantages owing to their multicomponent synergism. Guipi Pill (GPP), a Ming Dynasty–documented formula from *Jisheng Fang*, has been used clinically for centuries to treat anxiety-related syndromes via its spleen-invigorating and mind-calming effects [1]. Modern studies have reported the effects of GPP in treating anorexia and depression, improving memory function, protecting from radiation, and promoting hematopoietic function [2–6].

GPP is composed of 11 Chinese herbs including honey-fried Radix Astragali, *Codonopsis pilosula*, *Angelica sinensis*, *Atractylodis macrocephala* Rhizoma stir-fried with wheat bran, Radix Aucklandiae, honey-fried licorice, fried Semen Zizyphi Spinosae, processed products of Polygalae Radix, *Poria cocos*, Longan Meat, and *Ziziphus jujuba* (enucleated). In the prescription, honey-fried Radix Astragali and *C. pilosula* are monarch drugs; *A. sinensis*, Longan Meat, *A. macrocephala* Rhizoma stir-fried with wheat bran and honey-fried licorice are ministerial medicines; fried Semen *Zizyphi Spinosae, P. cocos*, processed products of Polygalae Radix, Radix Aucklandiae, and *Z. jujuba* are adjuvant drugs; honey-fried licorice is a medicinal preparation that has the function of harmonizing various medicinal materials. This classic formula exerts its therapeutic effects through multicomponent synergistic actions that holistically regulate the neuroendocrine-immune network [7–9]; however, the complex chemical composition of this formulation has precluded complete elucidation of the pharmacologically active compounds, particularly with respect to the systematic characterization of their in vivo metabolic processes and pharmacokinetic profiles. Current studies face the following three critical challenges: First, conventional methods of analyses cannot comprehensively capture the dynamic metabolic processes of complex formulae in vivo and particularly lack synchronized analyses across multiple matrices including the blood, urine, bile, and feces. Second, the heterogeneity of structurally diverse active constituents (e.g., highly polar flavonoid glycosides vs. lipophilic terpenoid lactones) during absorption, distribution, metabolism, and excretion remains unquantified. Third, pharmacologically active novel compounds generated through metabolic pathways demonstrating development potential have not been adequately explored. These knowledge gaps indicate the lack of the extent of GPP-related research, thereby limiting its precise clinical applications [10–12].

To overcome these bottlenecks, high-resolution mass spectrometry (HRMS) was innovatively integrated with multidimensional pharmacokinetic strategies in the current study. UHPLC-Q-Orbitrap-MS was employed for integrated quad-matrix metabolic profiling (blood, urine, bile, feces) in rats following the oral administration of GPP, whereas synchronous UHPLC-MS/MS multicomponent monitoring methods were established for the quantitative pharmacokinetic evaluation of the six characteristic prototype compound categories. By systematically tracking Phase I and Phase II metabolic reaction pathways, a comprehensive in vivo metabolic network of GPP was constructed. Our findings not only systematically elucidate the metabolic fate of this classical formula but also establish a methodological foundation for the in-depth analyses of the pharmacologically active substance bases in other TCM formulae.

2 | Experimental

2.1 | Materials and Chemicals

GPP (concentrated pills) was purchased from the manufacturer Jiuzhitang Co., Ltd. (batch No. 202003020 [Changsha, China]). The 18 reference standards are shown in Table S1.

LC-MS grade methanol and acetonitrile were purchased from Sigma-Aldrich (St. Louis, MO, USA), and LC-MS grade formic acid was purchased from Fisher Scientific (Fair Lawn, NJ, USA). Purified water was obtained from Wahaha Co. Ltd. (Hangzhou, China).

2.2 | Instruments and Analytical Conditions

2.2.1 | Qualitative Analysis

The UHPLC-MS/MS system consisted of a Vanquish Flex Ultra-high performance liquid chromatography system coupled with a Q-Exactive Orbitrap mass spectrometer (Thermo Fisher Scientific, MA, USA). An ACQUITY UHPLC BEH C_{18} column (100 mm × 2.1 mm × 1.7 μm) and an electrospray ionization (ESI) source were used for all analyses.

Mobile phase A (0.1% formic acid in water) and B (acetonitrile) were used for gradient elution as follows: 0–14.5 min, 10%–27% B; 14.5–16 min, 27%–38% B; 16–21 min, 38%–62.5% B; 21–31 min, 62.5%–100% B; 31–31.1 min, 100%–10% B; 31.1–34.1 min, 10% B. The flow rate was 0.2 mL/min, column temperature was 35°C, injection volume was 5 μL, sheath flow rate was 30 arb, auxiliary flow rate was 10 arb, spray voltage in the ESI^+ mode was 3.8 kV and in the ESI^- mode was 3.0 kV, capillary temperature was 320°C, and the auxiliary gas temperature was 310°C in the positive ion mode and 350°C in the negative ion mode. The data acquisition mode was full MS-$ddMS^2$ (TopN, $N = 10$), the scanning range was 100.0–1500.0 *m/z*, the collisional gas was nitrogen, and the collision energies (CEs) were 20, 40, and 60 eV. Both positive and negative ion modes were used for analysis.

TraceFinder 4.1 General Quan data processing system and Xcalibur 2.1 workstation were used for data acquisition and processing. The molecular formula of metabolites was inferred using Xcalibur 2.1 within the mass deviation of 5 ppm. The prototype components in samples were rapidly screened and identified based on the results from the chemical composition analysis of GPP in our laboratory. In addition, by consulting the literature related to the chemical composition of GPP, a metabolite database containing the compound name, molecular formula, accurate molecular weight, and primary and secondary MS data was established to rapidly screen and identify the metabolites of GPP in rats.

2.2.2 | Quantitative Analysis

An ExionLC AD UHPLC system coupled with AB SCIEXQTRAP 5500 tandem mass spectrometry (AB SCIEX, Framingham, MA, USA) was used for analysis. The mobile phase consisted of solvent A (0.1% formic acid) and solvent B (acetonitrile), which were used for gradient elution: 1–2 min 5%–20% B; 2–5 min 20%–60% B; and 5–8 min 60%–95% B at a flow rate of 0.4 mL/min. The conditions used for MS were as follows: ESI source: curtain gas, 35 L/min; collision gas, medium/9; ion-spray voltage, 4.5 kV/−3.5 kV; temperature, 550°C; ion source Gas 1, 50 L/min; ion source Gas 2, 55 L/min. Multiple reaction monitoring in the positive and negative ion mode was used, and the optimized transitions, CE, and declustering potential are shown in Table 1.

TABLE 1 | The optimal MRM quantification parameters of six analytes and IS.

Name	t_R (min)	Precursor ion	Product ion	Declustering potential (V)	Collision energy (eV)
Liquiritin	3.56	417.0 $[M-H]^-$	255.0	−120	−28
Ligustilide	6.53	191.4 $[M+H]^+$	117.2	110	29
Costunolide	6.64	233.2 $[M+H]^+$	187.2	92	20
Dehydrocostus lactone	6.77	231.2 $[M+H]^+$	185.2	98	22
Atractylenolide I	7.27	231.3 $[M+H]^+$	185.0	144	28
Glycyrrhetinic acid	7.49	469.1 $[M-H]^-$	425.4	−29	−67
Acetylsalicylic acid	3.96	179.0 $[M-H]^-$	137.0	−20	−14
Diazepam	5.06	285.2 $[M+H]^+$	193.2	93	28

2.3 | Sample Preparation

2.3.1 | Preparation of Samples for Qualitative Analysis

Twelve specific-pathogen-free (SPF) male Sprague Dawley (SD) rats weighing 180–220 g (Animal ethics No. SYPU-IACUC-S2021-06.18-201) were used in this study. The SD rats were purchased and raised in the Animal Experimental Center of Shenyang Pharmaceutical University, housed at a temperature of 22 ± 2°C and 50%–60% humidity, and subjected to a 12-h/12-h light/dark cycle. All experiments were conducted in accordance with the animal experiment guidelines of Shenyang Pharmaceutical University. All experimental protocols were approved by the institution's Animal Ethics Committee.

The rats were fasted for 12 h but provided access to drinking water ad libitum before commencing experiments. The animals were randomly divided into a control, plasma, bile, or urine/feces groups ($n = 3$). At 8:00 a.m., GPP was administered at a dose of 1.26 g/kg for 3 days. GPP was dissolved in purified water and administered as an oral solution (0.1 g/mL). Rats in the control group were administered an equivalent volume of normal saline.

Plasma samples were collected from the orbital venous plexus of rats at 0.17, 0.33, 0.5, 1, 2, 3, 5, 7, 9, and 12 h after the last oral administration, placed in a centrifuge tube with heparin, and centrifuged at 4000 × *g* for 10 min. Plasma samples (50 μL) obtained from 3 rats at different time points were mixed to yield a mixed plasma sample. Next, 3 mL of methanol was added to 1 mL of the mixed plasma sample to precipitate the proteins. The sample was centrifuged at 12 000 × *g* for 10 min at 4°C, and the supernatant was dried in a stream of nitrogen at 30°C. The residue was redissolved in 100 μL of 70% acetonitrile, centrifuged, and analyzed.

After anesthesia with pentobarbital sodium, bile samples from rats in the bile group were collected for 0–2, 2–4, 4–8, 8–12, 12–24, and 24–36 h by bile duct intubation. Next, 2 mL of methanol was added to 1 mL of the mixed sample for treatment. The subsequent steps were identical to those used for plasma pretreatment, except that 1 mL of 50% acetonitrile was used as the enrichment solvent [13].

Urine samples of rats were collected in a manner similar to that used for bile samples. The subsequent steps were identical to those for bile pretreatment, except that the 200 μL of 50% acetonitrile was used as the enrichment solvent.

Fecal samples were collected in a manner similar to that used for urine samples. The mixed fecal sample (0.5 g) was extracted using ultrasonication for 30 min using 2.5 mL of 50% methanol. The subsequent steps were similar to those used for bile pretreatment.

2.3.2 | Preparation of Plasma Samples for Quantitative Analysis

Twelve male SPF SD rats weighing 220–250 g (Animal ethics No. SYYXY2022110201) were purchased and raised in the SPF experimental animal center of Shenyang Medical College. The rats were housed at a temperature of 22 ± 2°C and humidity of 50%–60%, and subjected to a 12-h/12-h light/dark cycle. All experiments were performed in accordance with the animal experiment guidelines of Shenyang Medical College, and all experimental protocols were approved by the institution's Animal Ethics Committee.

Before administration, the rats were fasted for 12 h but allowed access to drinking water ad libitum. Before administration (0 h) and after administration (2.52 g/kg) for 0.083, 0.167, 0.333, 0.5, 1, 2, 4, 6, 8, 10, 12, 24, 36, and 48 h, blood from the eye orbits was placed in a heparinized centrifuge tube and centrifuged at 3500 × *g* for 10 min. To the upper plasma layer, 10 μL of the internal standard (IS) was added, followed by the addition of 100 μL of plasma. Next, 300 μL of methanol was added to precipitate proteins. Then, 1 mL of ethyl acetate was added and the sample was ultrasonicated for 5 min and centrifuged at 12 000 × *g* for 10 min at 4°C. Lastly, 1 mL of the supernatant was dried in a gentle stream of air, redissolved in 100 μL of acetonitrile, ultrasonicated, and centrifuged.

2.4 | Preparation of Standard Solutions for Qualitative Analysis

The reference substances of the 18 compounds were accurately weighed and dissolved in methanol to obtain a stock solution. The

stock solution was diluted with 70% methanol to about 0.2 μg/mL and used as the mixed reference solution.

2.5 | Preparation of the Calibration Standard and Quality Control Samples

The reference substances of six compounds were accurately weighed and dissolved in methanol to obtain the stock solution of each substance. The stock solutions of each substance were mixed to yield a mixed stock having a final concentration of 80.00 μg/mL liquiritin, 57.00 μg/mL ligustilide, 27.50 μg/mL costunolide, 80.00 μg/mL dehydrocostus lactone, 38.00 μg/mL atractylenolide I, and 86.00 μg/mL glycyrrhetinic acid. The mixed stock solution of the IS was prepared following the same method. The concentration was 5.400 μg/mL of acetylsalicylic acid and 1.200 μg/mL of diazepam.

The standard solutions (10 μL each) and 10 μL of the IS solution were added to 100 μL of blank plasma to obtain seven simulated plasma samples with different concentration gradients, which were used to construct the respective standard curves. The final simulated plasma concentration gradients of these six substances were 3.200, 12.80, 25.60, 64.00, 160.0, 400.0, and 800.0 ng/mL liquiritin; 2.280, 9.120, 18.24, 45.60, 114.0, and 285.0 ng/mL ligustilide; 1.100, 4.400, 8.800, 22.00, 55.00, 137.5, and 275.0 ng/mL costunolide; 3.200, 12.80, 25.60, 64.00, 160.0, 400.0, and 800.0 ng/mL dehydrocostus lactone; 1.520, 6.080, 12.16, 30.40, 76.00, 190.0, and 380.0 ng/mL atractylenolide I; and 3.440, 13.76, 27.52, 68.80, 172.0, 430.0, and 860.0 ng/mL glycyrrhetinic acid. Quality control (QC) samples of low, medium, and high concentrations obtained using the same method included 8.000, 240.0, and 560.0 ng/mL liquiritin; 5.700, 171.0, and 399.0 ng/mL ligustilide; 2.750, 82.50, and 192.5 ng/mL costunolide; 8.000, 240.0, and 560.0 ng/mL dehydrocostus lactone; 3.800, 114.0, and 266.0 ng/mL atractylenolide I; and 8.600, 258.0, and 602.0 ng/mL glycyrrhetinic acid.

3 | Results

3.1 | Qualitative Analysis

In the previous experiment [8], 116 chemical components of GPP were identified in vitro. On this basis, a total of 106 compounds were identified, including 48 prototype components and 58 possible metabolites. Among them, MC2, MC3, MC5, MC11, MC26, MF1, MF2, MF3, and MF4 were presumed to be novel compounds. Figure 1 shows the total ion current (TIC) chromatogram for plasma, bile, urine, and feces after deducting the blank reading in the positive and negative ion modes, and Tables S2 and S3 present specific information on the prototypes and metabolites.

3.1.1 | Phenylpropanoids

Among the prototype components, compounds 3,4,5-trimethoxycinnamic acid (N49) and coumarin (N72) were determined to be phenylpropanoids. Four coumarin metabolites were detected in the plasma, bile, feces, and urine. Coumarin mainly undergoes Phase I metabolism (hydration, reduction, and oxidation) and conjugation reaction (methylation).

Based on the literature, MA1–MA4 were speculated to be the metabolites of coumarin (N72) [14]. The excimer ion peak of MA1 is 18 Da more than that of the prototype. In the secondary fragment, *m/z* 147.044 22 is the fragment produced by the loss of a water molecule from MA1. The fragment *m/z* 91.054 76 is consistent with that of the prototype. It is speculated that the fragment corresponds to the intramolecular hydration metabolite of coumarin, which may be due to the introduction of a water molecule at the double bond in the coumarin ring. The excimer ion peak of MA2 is 2 Da more than that of the prototype, the *m/z* 131.049 62 $[M+H\text{-}H_2O]^+$ fragment in the secondary fragment is 2 Da more than that of the prototype, and the *m/z* 103.054 80 fragment is consistent with the prototype. Based on these findings, the generated compound was speculated to be the metabolite resulting from the reduction of the ketone moiety in coumarin to alcohol. The excimer ion peak of MA3 is 16 Da more than that of the prototype, and the *m/z* 107.085 75 $[M+H\text{-}C_2H_4O_2]^+$ in the secondary fragment is 16 Da more than that of the prototype. It was speculated that the product is the metabolite resulting from the oxidation of the aromatic ring of coumarin. The excimer ion peak of MA4 is 14 Da more than that of the prototype, and it has the same fragments *m/z* 103.054 79 and *m/z* 91.054 87 as the prototype, suggesting it to be the methylated metabolite of coumarin.

3.1.2 | Flavones and Their Glycosides

Prototypes of flavonoids and their glycosides such as spinosin (N33), liquiritigenin (N48), glycitein (N52), calycosin (N53), isoliquiritigenin (N70), formononetin (N71), licoisoflavone A (N88), and licoisoflavone B (N97), and 12 metabolites of flavonoids and their glycosides were detected in the biological samples. As flavonoids and their glycosides have similar parent nuclear structures, they have similar metabolic pathways. Oxidation, reduction, heterocyclic cracking, and deglycosylation were the main reactions in Phase I metabolism, whereas glucuronidation and sulfation were the main reactions in Phase II metabolism.

MB1–MB5 are metabolites of liquiritin (N34). Liquiritin is typically absorbed by the body after deglucosylation as liquiritigenin (MB2) or isoliquiritigenin (MB5), and then remetabolized in vivo to liquiritin [15, 16]. The molecular weight of MB1 is 80 Da higher than that of the parent compound, suggesting it to be the sulfated conjugate of liquiritin. MB3 and MB4 have a molecular weight 16 Da higher than that of the parent compound, suggesting them to be oxidative metabolites of liquiritin with two different oxidation sites. Based on the literature, oxidation is favored on the A ring of MB3 and the B ring of MB4. MB6, and MB9 exhibited the same characteristic fragments as (iso)liquiritigenin, with a difference of 176 Da in their precursor ion peaks, suggesting them to be the glucuronidated metabolites of (iso)liquiritigenin. MB7 and MB10 shared identical characteristic fragments with (iso)liquiritigenin, with a difference of 80 Da in their precursor ion peaks, suggesting they are sulfated metabolites of (iso)liquiritigenin. MB8 and MB12 showed precursor ion peaks 2 Da higher than that of (iso)liquiritigenin, implying they are the

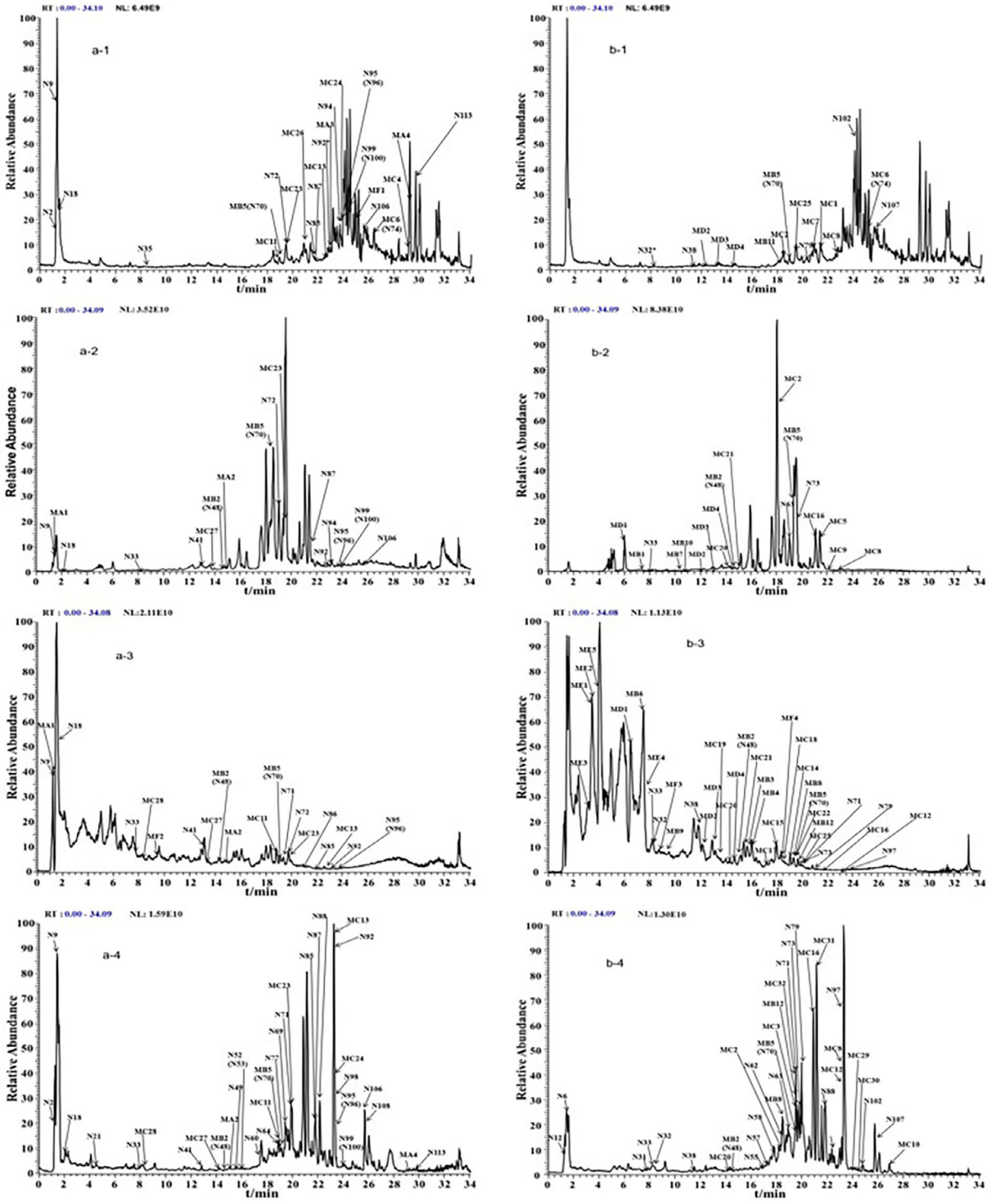

FIGURE 1 | Total ion current (TIC) chromatogram with subtract background (1) plasma (2) bile (3) urine (4) feces (a: positive ion mode; b: negative ion mode).

reduced metabolites of (iso)liquiritigenin. The possible metabolic pathways are shown in Figure 2.

3.1.3 | Terpenoids and Their Glycosides

Terpenoids and their glycoside components are a major class of chemical constituents in GPP. Sixteen prototype components including tenuifolin (N63), poricoic acid E (N64), astragaloside IV (N69), and glycyrrhizic acid (N73) were identified in vivo. A total of 32 terpenoid and glycoside metabolites including MC1–MC32 were detected in the plasma, bile, feces, and urine, among which MC2, MC3, MC5, MC11, and MC26 were presumed to be novel compounds. Specific metabolic profiles are listed in Table S2.

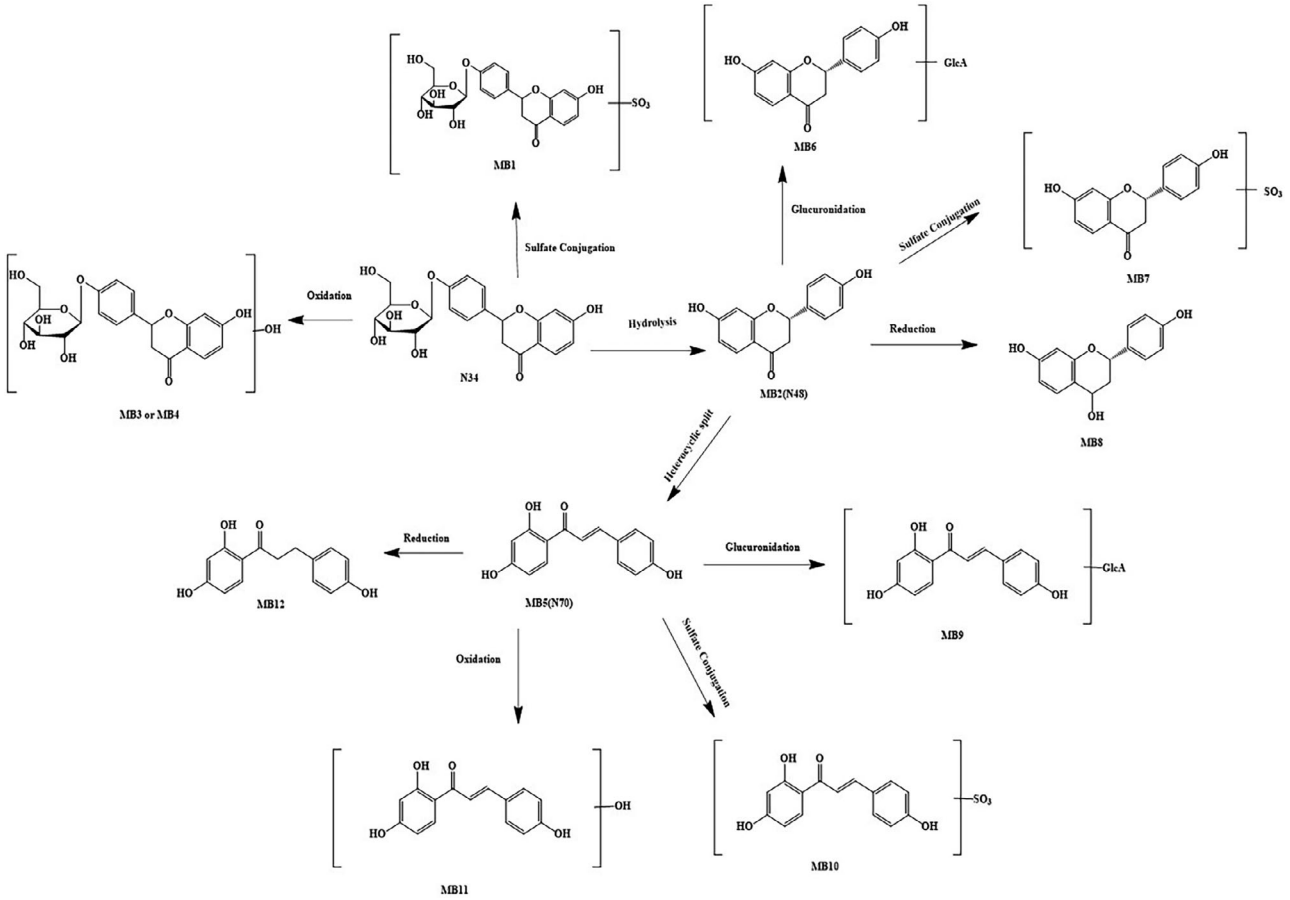

FIGURE 2 | Metabolic pathways of liquiritin.

MC1–MC3 are metabolites of tenuifolin saponin (N63). As triterpenoid saponins typically undergo glycoside hydrolysis and enter the systemic circulation in the form of aglycones, the fragmentation patterns of tenuifolin metabolites were analyzed using the two novel compounds MC2 and MC3 as examples. MC1 has a molecular weight 162 Da lower than that of the prototype compound, suggesting it to be the glycoside-hydrolyzed metabolite of tenuifolin according to the literature [17]. MC2 exhibits a retention time of 18.55 min and a quasi-molecular ion peak $[M\text{-}H]^-$ at *m/z* 531.299 62, corresponding to a proposed molecular formula of $C_{30}H_{44}O_8$. The 14 Da higher precursor ion compared with that of MC1 indicates it to be the oxidized metabolite of tenuifolin, where the primary alcohol was converted to a carboxylic acid following glycoside hydrolysis. This hypothesis was supported by structural modeling using ChemDraw, with key fragment ions observed at *m/z* 486.294 16$[M\text{-}H\text{-}CHO_2]^-$, 463.289 86$[M\text{-}H\text{-}C_5H_8]^-$, and 339.889 77$[M\text{-}H\text{-}C_5H_8\text{-}C_7H_9O_2]^-$. MC2 was confirmed as an oxidized derivative of MC1 based on these fragments. The mass spectrum and fragmentation pattern of MC2 are shown in Figure 3A. MC3 had a retention time of 19.27 min and a quasi-molecular ion peak $[M\text{-}H]^-$ at 519.334 59, indicating its molecular formula to be $C_{30}H_{48}O_7$. The quasi-molecular ion peak of MC3 is 2 Da larger than that of MC1, indicating the former to be a metabolite of tenuifolin resulting from the reduction of the double-bond following sugar hydrolysis. The fragmentation pathway of MC3 was simulated using ChemDraw. Fragment ions were observed at *m/z* 457.330 08$[M\text{-}H\text{-}CH_2O_3]^-$, 444.150 91$[M\text{-}H\text{-}CH_2O_3\text{-}CH_3]^-$, 423.288 64$[M\text{-}H\text{-}C_7H_{11}]^-$, and 351.268 83$[M\text{-}H\text{-}C_7H_{11}\text{-}C_3H_4O_2]^-$, supporting the identification of MC3 as a metabolite resulting from the reduction of the double bond. The mass spectrum and fragmentation pattern of MC3 are shown in Figure 3B.

MC4 and MC5 are metabolites of astragaloside IV (N69). The novel compound MC5 was used as an example to analyze the fragmentation patterns of the metabolites of astragaloside IV. MC4 has a molecular weight 294 Da lower than that of astragaloside IV, with a quasi-molecular ion peak $[M+H]^+$ at 491.374 02. Fragment ions were observed at *m/z* 461.066 96$[M+H\text{-}CH_2O]^+$, 443.627 90$[M+H\text{-}CH_2O\text{-}H_2O]^+$, 387.605 90$[M+H\text{-}CH_2O\text{-}H_2O\text{-}C_3H_4O]^+$, 354.078 49$[M+H\text{-}C_5H_{12}O_4]^+$, and 313.434 30$[M+H\text{-}C_8H_{17}O_4]^+$, suggesting MC4 to be cycloastragenol, the aglycone metabolite resulting from the hydrolysis of the sugar. MC5 has a retention time of 21.93 min and exhibits a quasi-molecular ion peak $[M\text{-}H]^-$ of 569.313 35. The proposed molecular formula of MC5 is $C_{30}H_{50}O_8S$. The molecular weight of MC5 is 80 Da higher than that of MC4, indicating MC5 to be the sulfated metabolite of astragaloside IV after the hydrolysis of this glycoside. The fragmentation pathway of MC5 was simulated using ChemDraw. Key fragment ions were observed at *m/z* 499.672 97$[M\text{-}H\text{-}C_4H_6O]^-$, 485.334 99$[M\text{-}H\text{-}C_4H_6O\text{-}CH_2]^-$, 410.492 31$[M\text{-}H\text{-}C_4H_6O\text{-}CH_2\text{-}C_3H_7O_2]^-$, and 299.971 44$[M\text{-}H\text{-}C_4H_6O\text{-}CH_2\text{-}C_3H_7O_2\text{-}C_7H_{11}O]^-$. Therefore, MC5 was speculated to be the sulfated metabolite of MC4. The mass spectrum and fragmentation pattern of MC5 are shown in Figure 3C.

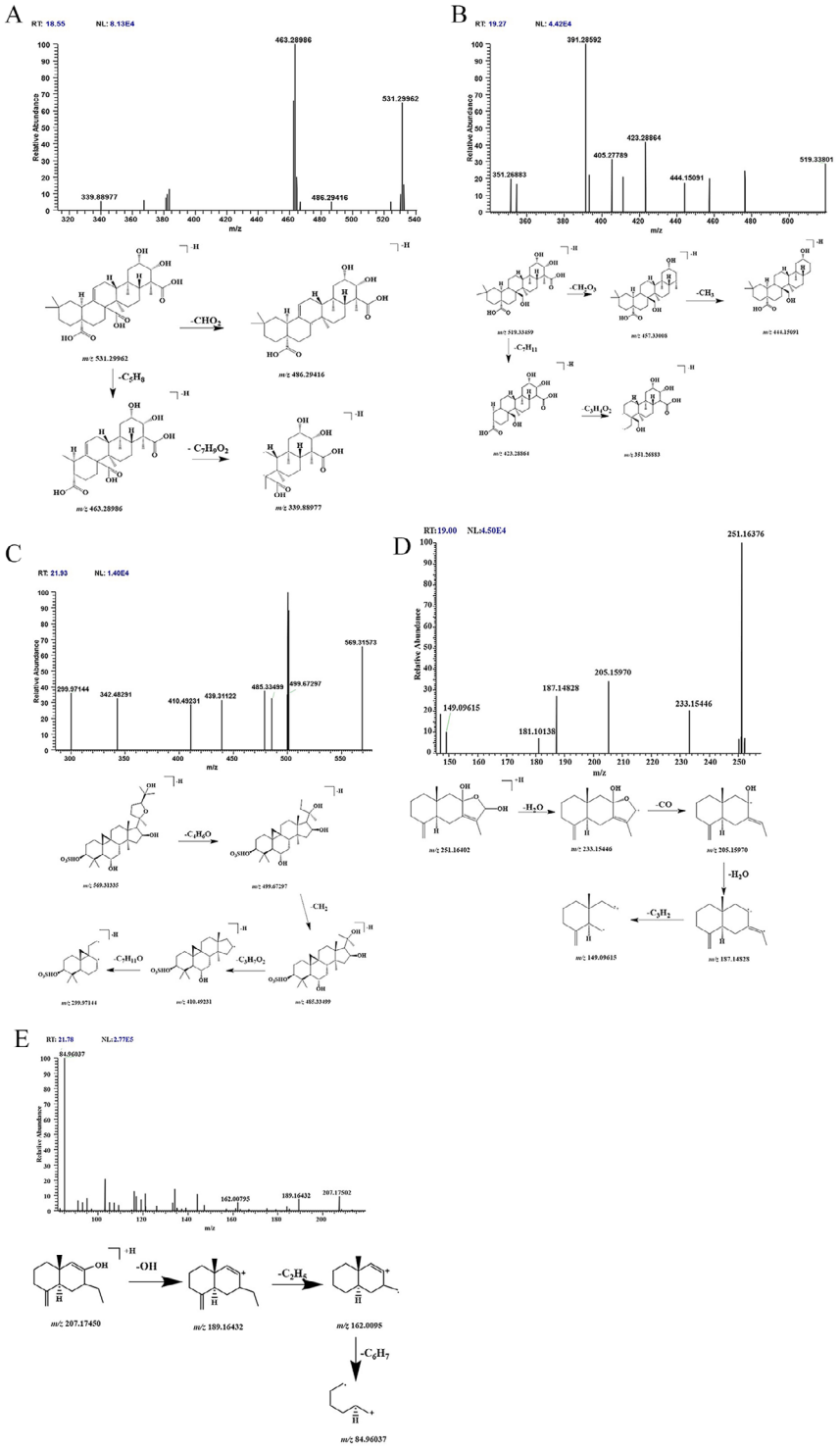

FIGURE 3 | MS^2 spectrum of MC2 (A)/MC3 (B)/MC5 (C)/MC11 (D)/MC26 (E) and proposed fragmental pathways.

MC11–MC22 are the metabolites of the sesquiterpenoid compound atractylenolide III (N86). Its primary metabolic pathways were found to include oxidation, reduction, demethylation, and hydration reactions in Phase I metabolism and glucuronidation and sulfation reactions in Phase II metabolism. The possible metabolic pathways are shown in Figure 4. The novel compound MC11 was used as an example to analyze the fragmentation patterns of the metabolites of atractylenolide III. MC11 has a retention time of 19.00 min and a quasi-molecular ion peak $[M+H]^+$ at 251.164 02. The proposed molecular formula is $C_{15}H_{22}O_3$. Its quasi-molecular ion peak is 2 Da higher than that of the prototype, suggesting it to be the reduced metabolite of atractylenolide III. The fragmentation pathway of MC11 was simulated using ChemDraw, and the fragment ions were identified to include *m/z* 205.159 70$[M+H-H_2O]^+$, 233.154 46$[M+H-H_2O-CO]^+$, 187.148 28$[M+H-H_2O-CO-H_2O]^+$, and 149.096 15$[M+H-H_2O-CO-H_2O-C_3H_2]^+$. Therefore, MC11 was speculated to be the reduced metabolite of atractylenolide III. The mass

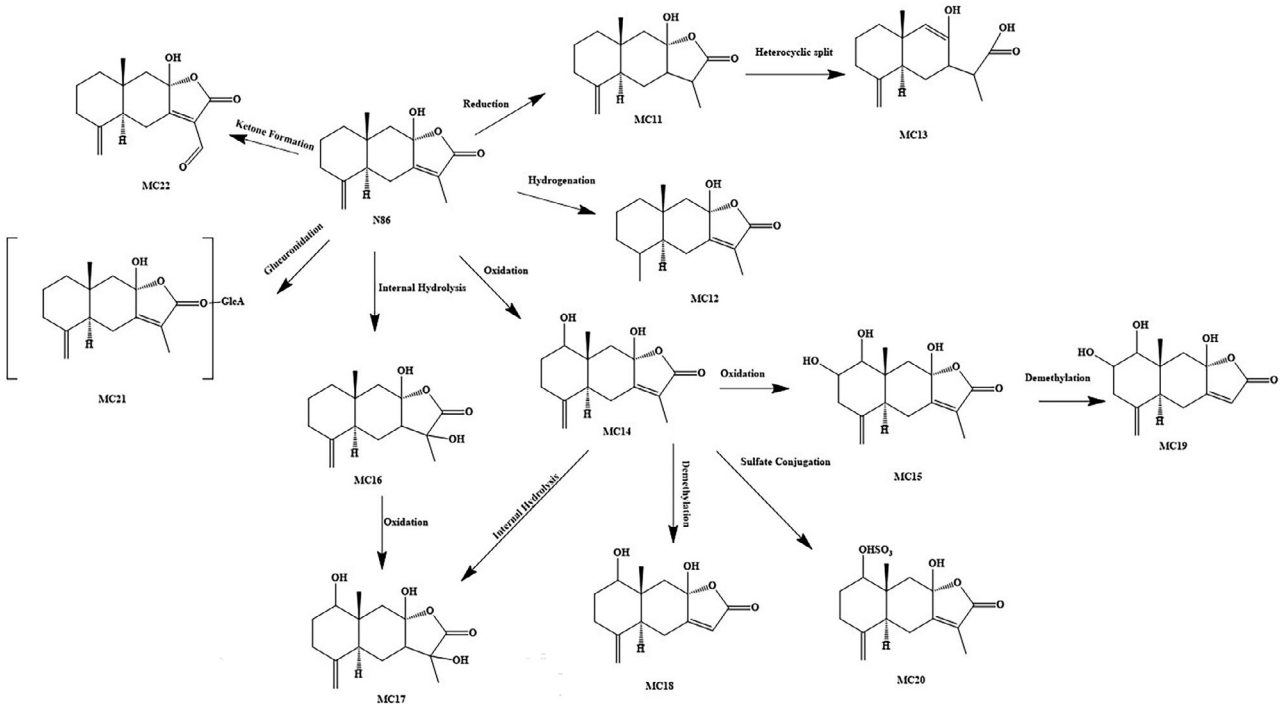

FIGURE 4 | Metabolic pathways of atractylenolide III.

spectrum and fragmentation pattern of MC11 are presented in Figure 3D.

MC25 and MC26 are metabolites of atractylenolide I (N99) primarily formed via multistep metabolic reactions. The novel compound MC26 was used as an example to analyze the fragmentation patterns of atractylenolide l metabolites. MC25 has a molecular weight 20 Da higher than that of the prototype, along with a characteristic fragment ion at *m/z* 205.159 33 $[M\text{-}H\text{-}COOH]^-$, suggesting it to be a metabolite of atractylenolide I resulting from heterocyclic ring cleavage and reduction reactions [18]. MC26 has a retention time of 21.78 min and a quasi-molecular ion peak $[M+H]^+$ at 207.174 34. The proposed molecular formula is $C_{14}H_{22}O$. Its molecular weight is 44 Da lower than that of MC25, indicating it as a decarboxylated metabolite of MC25. The fragmentation pathway of MC26 was simulated using ChemDraw, and the key fragment ions were identified at *m/z* 189.164 32$[M+H\text{-}OH]^+$, 162.007 95$[M+H\text{-}OH\text{-}C_2H_5]^+$, and 84.960 37$[M+H\text{-}OH\text{-}C_2H_5\text{-}C_6H_7]^+$. Therefore, MC26 was speculated to be the decarboxylated metabolite of atractylenolide I based on heterocyclic ring cleavage and reduction reactions. The mass spectrum and fragmentation pattern of MC26 are shown in Figure 3E.

3.1.4 | Volatile Oils

Volatile oil components, primarily derived from *A. sinensis*, are a major class of components in GPP present in high concentrations. Seven prototype compounds of volatile oils including senkyunolide H (N41), ligustilide (N92), and cinnamaldehyde (N113), along with four related metabolites were identified in vivo. MD1 and MD2 are the metabolites of senkyunolide H (N41), and their MS/MS spectra are consistent with those reported in the literature [19]. MD1 has a molecular weight 80 Da higher than that of the prototype, suggesting it is a sulfated metabolite of senkyunolide H. The quasi-molecular ion peak of MD2 and its characteristic fragment *m/z* 221.081 53 $[M\text{-}H\text{-}C_5H_8O]^-$ are both 2 Da lower than those of MD1, indicating it to be the dehydrogenated metabolite of MD1. MD3 and MD4 are metabolites of ligustilide (N92) and have MS/MS spectra consistent with those reported in the literature [20]. MD3 has a molecular weight 96 Da higher than that of the prototype. Based on the literature, MD3 was speculated to be the sulfated metabolite of ligustilide resulting from oxidation. MD4 has a molecular weight 2 Da lower than that of MD3, suggesting it to be a metabolite of MD3 resulting from the reduction of the double bond.

3.1.5 | Organic Acids

Six organic acid compounds including quinic acid (N6), isoferulic acid (N31), and ferulic acid (N32) along with five related metabolites, were identified in vivo. ME1–ME3 are the metabolites of ferulic acid (N32) and have MS/MS spectra consistent with those reported in the literature [21, 22]. ME1 has a molecular weight 57 Da higher than that of the prototype, and its fragment ion *m/z* 193.047 55 ([M-glycine]) matched the quasi-molecular ion peak of the prototype, suggesting it to be the glycine-conjugated metabolite of ferulic acid. ME2 has a molecular weight 80 Da higher than that of the prototype, and its fragment ions *m/z* 193.04755 and 134.03726 match the quasi-molecular ion peak of the prototype, suggesting it to be the sulfated metabolite of ferulic acid. ME3 has a molecular weight 2 Da higher than that of ME2, consistent with the double bond-reduced metabolite of ME2.

ME4 and ME5 are metabolites of p-hydroxybenzoic acid (N38), with MS/MS spectra consistent with those reported in the litera-

ture [23]. ME4 has a molecular weight 28 Da higher than that of the prototype, suggesting it to be the dimethylated metabolite of p-hydroxybenzoic acid. ME5 has a molecular weight 28 Da higher than that of ME4, suggesting it to be the methylated metabolite of ME4 resulting from hydroxylation.

3.1.6 | Alkynyl Glycosides

Codonopsis alkynyl glycoside, the primary active constituent of *C. pilosula*, is an alkynyl glycoside that typically undergoes hydrolysis and enters systemic circulation in the form of an aglycone for metabolism. Four potentially novel compounds MF1–MF4 were detected in plasma and urine samples. Specific information on the metabolites is shown in Table S2. The fragmentation patterns of compounds MF1–MF4 are as follows:

MF1 has a retention time of 24.14 min and a quasi-molecular ion peak $[M+H]^+$ at 235.132 87. The proposed molecular formula is $C_{14}H_{18}O_3$. Its molecular weight was 185 Da lower than that of codonopsis alkynyl glycoside, suggesting it to be the hydrolysis metabolite of codonopsis alkynyl glycoside. The fragmentation pathway of MF1 was simulated using ChemDraw and the key fragment ions were observed at *m/z* 217.122 65 $[M+H\text{-}H_2O]^+$, 179.070 39 $[M+H\text{-}H_2O\text{-}C_3H_2]^+$, 165.055 21 $[M+H\text{-}H_2O\text{-}C_3H_2\text{-}CH_2]^+$, 133.065 11 $[M+H\text{-}H_2O\text{-}C_3H_2\text{-}CH_2\text{-}H_2O_2]^+$, 105.070 37 $[M+H\text{-}H_2O\text{-}C_3H_2\text{-}CH_2\text{-}H_2O_2\text{-}C_2H_4]^+$, and 91.054 89 $[M+H\text{-}H_2O\text{-}C_3H_2\text{-}CH_2\text{-}H_2O_2\text{-}C_2H_4\text{-}CH_3]^+$. The mass spectrum and fragmentation pattern of MF1 are shown in Figure 5A.

MF2 has a retention time of 9.05 min and exhibits a quasi-molecular ion peak $[M+H]^+$ at 219.137 96. The proposed molecular formula is $C_{14}H_{18}O_2$. Its molecular weight was 16 Da lower than that of MF1, suggesting it to be the alcohol-reduced metabolite of MF1. The fragmentation pathway of MF2 was simulated using ChemDraw, and the key fragments ions were observed at *m/z* 201.127 78 $[M+H\text{-}H_2O]^+$, 173.096 97 $[M+H\text{-}H_2O\text{-}OH]^+$, 157.068 37 $[M+H\text{-}H_2O\text{-}OH\text{-}C_2H_5]^+$, 129.073 64 $[M+H\text{-}C_7H_7]^+$, 115.058 06 $[M+H\text{-}C_7H_7\text{-}CH_3]^+$, and 81.070 50 $[M+H\text{-}H_2O\text{-}OH\text{-}C_2H_5\text{-}C_6H_5]^+$. Therefore, MF2 was speculated to be the alcohol-reduced metabolite of codonopsis alkynyl glycoside, resulting from hydrolysis. The mass spectrum and fragmentation pattern of MF2 are shown in Figure 5B.

MF3 has a retention time of 8.48 min and exhibits a quasi-molecular ion peak $[M\text{-}H]^-$ at 263.091 40. The proposed molecular formula is $C_{14}H_{16}O_5$. Its molecular weight is 30 Da higher than that of MF1, suggesting it to be an ω-position oxidative metabolite of MF1. The fragmentation pathway of MF3 was simulated using ChemDraw, and the key fragment ions were observed at *m/z* 219.100 94 $[M\text{-}H\text{-}COOH]^-$, 203.068 74 $[M\text{-}H\text{-}COOH\text{-}OH]^-$, 177.089 97 $[M\text{-}H\text{-}COOH\text{-}OH\text{-}C_2H_4]^-$, 135.081 56 $[M\text{-}H\text{-}COOH\text{-}OH\text{-}C_2H_4\text{-}C_2H_4O]^-$, and 96.960 01 $[M\text{-}H\text{-}COOH\text{-}OH\text{-}C_2H_4\text{-}C_2H_4O\text{-}C_3H_6]^-$. Therefore, it was speculated to be a metabolite wherein the functional group at the ω-position of the codonopsis alkynyl glycoside was oxidized to carboxylic acid based on hydrolysis. The mass spectrum and fragmentation pattern of MF3 are shown in Figure 5C.

MF4 has a retention time of 18.27 min and a quasi-molecular ion peak $[M\text{-}H]^-$ at 249.112 14. The proposed molecular formula is $C_{14}H_{18}O_4$. Its molecular weight is 16 Da higher than that of MF1, suggesting it to be the alcohol-oxidation metabolite of MF1. The fragmentation pathway of MF4 was simulated using ChemDraw, and the key fragment ions were observed at *m/z* 195.617 89 $[M\text{-}H\text{-}C_4H_8]^-$ and 181.123 37 $[M\text{-}H\text{-}C_4H_8\text{-}OH]^-$. Therefore, MF4 was speculated to be the alcohol-oxidation metabolite of codonopsis alkynyl glycoside based on hydrolysis. The mass spectrum and fragmentation pattern of MF4 are presented in Figure 5D.

3.2 | Quantitative Analysis

3.2.1 | Method Validation

Selectivity was assessed by comparing the chromatograms obtained using identical analytical conditions for blank plasma, blank plasma spiked with the mixed standard solution and the IS, plasma samples collected from rats 1 h after the oral administration of GPP, and samples spiked with the IS. All plasma samples were processed following the method described in Section 2.3.2. The endogenous plasma components did not interfere significantly with the detection of any of the target analytes or the IS. Representative chromatograms are shown in Figure 6. Carryover was evaluated by injecting a processed blank plasma sample immediately after the injection of a sample at a concentration corresponding to the upper limit of quantification. The carryover for all six target analytes in the subsequent blank injection was < 20% of the lower limit of quantification (LLOQ). In addition, any observed carryover signal was < 5% of the response of the IS. Linearity was assessed by preparing calibration standards using blank rat plasma. This involved spiking the plasma with the mixed standard solution at seven concentrations. Calibration curves were constructed by plotting the peak area ratio (Y) of the analyte to the IS versus the nominal concentration (X) of the analyte in the plasma. Linear regression analysis was used to determine the regression equation for each analyte. The correlation coefficient (r) for all standard curves was > 0.99. The lowest concentration point on the calibration curve was defined as the LLOQ. Detailed information for each analyte, including the standard curve equation, linear range, and experimentally determined LLOQ, is summarized in Table 2.

Precision and accuracy were evaluated using QC samples at three concentration levels. The measured concentration of each QC sample was determined using the standard curve generated on the same day. The results (Table S4) demonstrated that the relative standard deviation for both intraday and interday precision was < 15%. The RE for accuracy was also < 15%. Extraction recovery (%) for each analyte was calculated using the formula (A/B) × 100%. The peak areas of the analytes obtained from QC samples (A) were compared with the peak areas obtained from the processed blanks spiked with the mixed standard solution. The matrix effect was assessed by comparing the mean peak area of an analyte in post-extraction-spiked samples (with the matrix) to the mean peak area of the analyte in neat standard solutions (without the matrix), and the results are presented in Table S4. The stability of the six target analytes

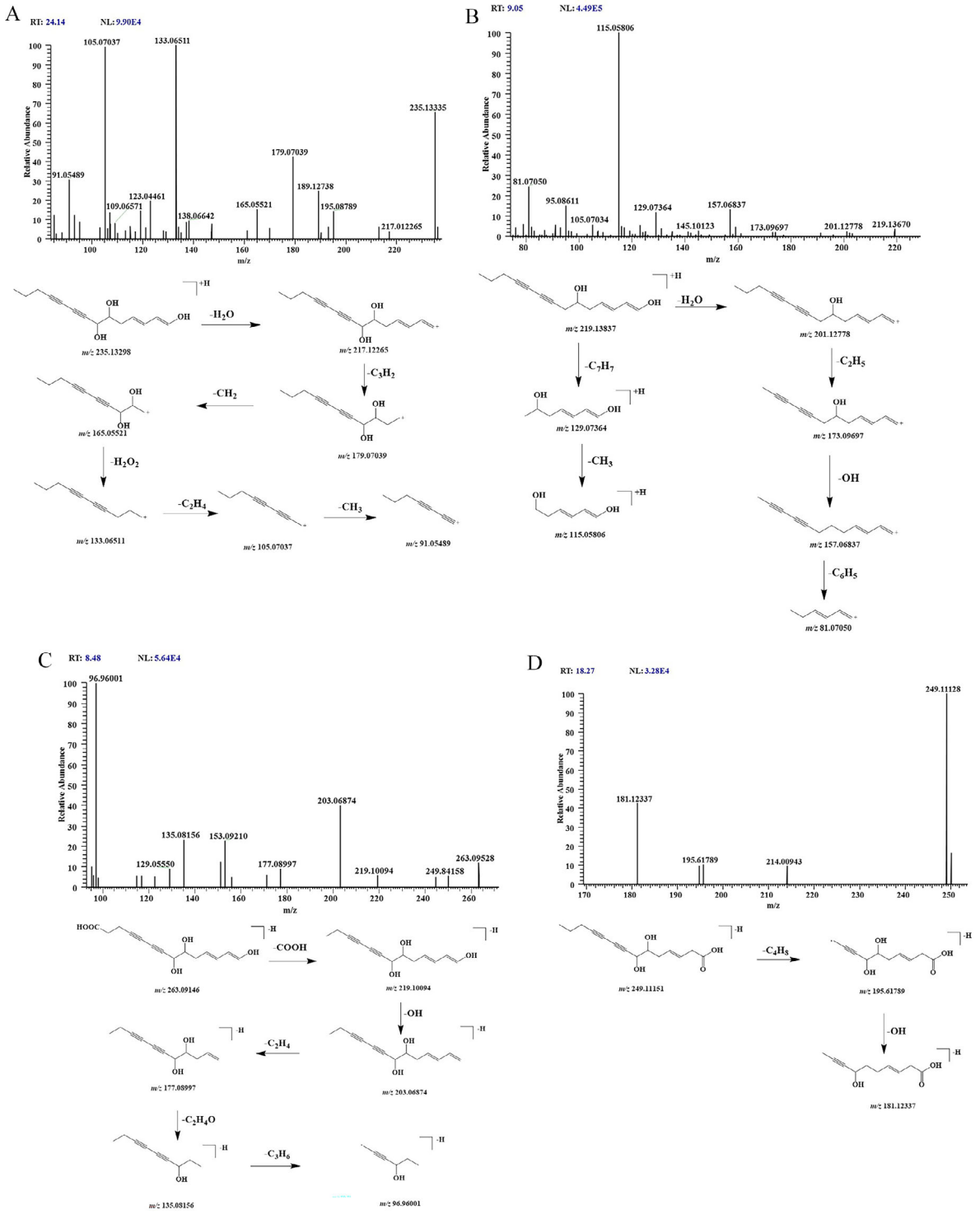

FIGURE 5 | MS^2 spectrum of MF1 (A)/MF2 (B)/MF3 (C)/MF4 (D) and proposed fragmental pathways.

in rat plasma was evaluated under the following conditions: storage of processed samples in the autosampler at 4°C for 24 h, storage at −20°C for 30 days, and storage after three complete freeze–thaw cycles. The freeze–thaw procedure consisted of: (1) Freezing at −20°C; (2) thawing at ambient temperature; (3) 24-h storage at 4°C. This cycle was repeated three times. All six analytes remained stable under these storage conditions (Table S5).

3.2.2 | Pharmacokinetic Results

Based on the previously established analytical method [24], the levels of the six markers in GPP were determined to be as follows: liquiritin 75.98 μg/g, ligustilide 1158.32 μg/g, costunolide 235.68 μg/g, dehydrocostus lactone 482.18 μg/g, atractylenolide I 4.98 μg/g, and glycyrrhetinic acid 12.12 μg/g. After oral administration, the peak areas recorded at each time point were applied to the

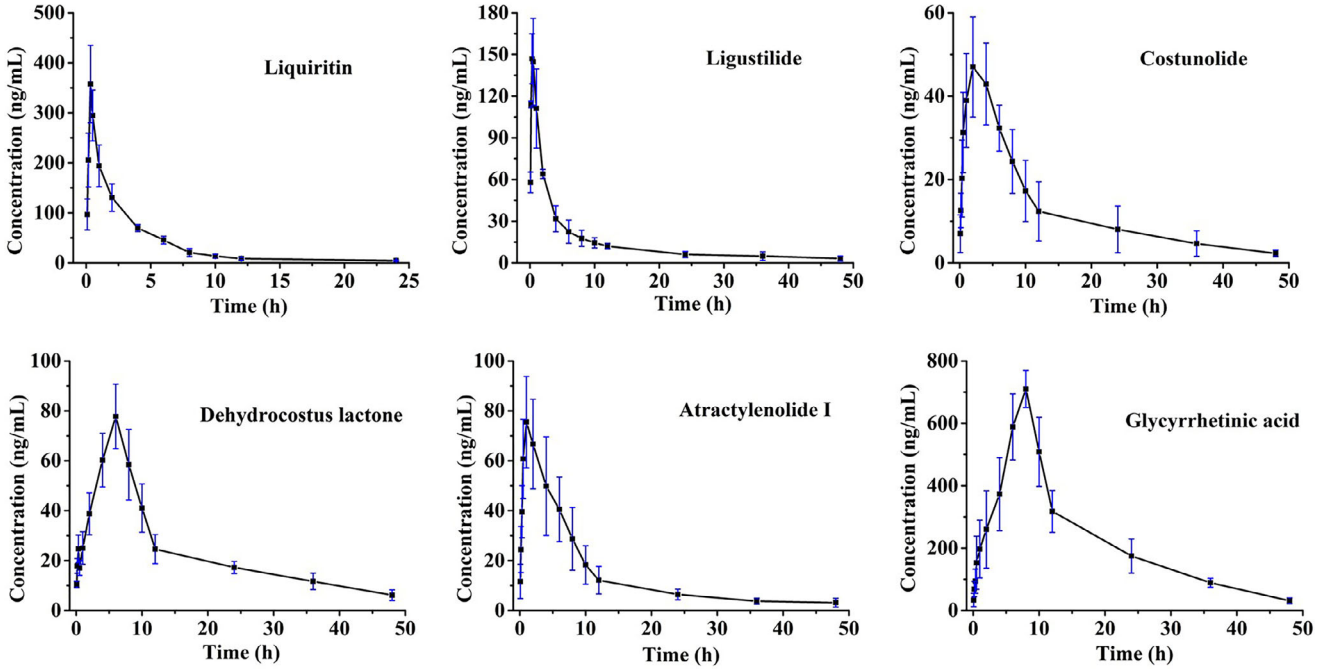

FIGURE 6 | Multiple reaction monitoring (MRM) chromatograms of the six compounds and IS from rat plasma: A: blank plasma; B: blank plasma spiked with the six analytes and IS; C: real plasma samples obtained from rat after oral administration of GPP.

TABLE 2 | The calibration curves, related coefficients, linear ranges, LLOQs of six analytes.

Analyte	Standard curves	Slope ± SE	Intercept ± SE	*r*	Linear ranges (ng/mL)	LLOQs (ng/mL, mean ± SD)	RSD%
Liquiritin	$y = 0.01299x + 0.01671$	0.01299 ± 0.00094	0.01671 ± 0.10763	0.9954	3.20–800.00	3.20 ± 0.23	3.29
Ligustilide	$y = 0.01105x + 0.14643$	0.01105 ± 0.00040	0.14643 ± 0.09740	0.9958	2.28–570.00	2.28 ± 0.43	6.32
Costunolide	$y = 0.05221x + 0.09465$	0.05221 ± 0.00093	0.09465 ± 0.10990	0.9983	1.10–275.00	1.10 ± 0.31	4.65
Dehydrocostus lactone	$y = 0.08714x + 0.07680$	0.08714 ± 0.00579	0.07680 ± 0.10451	0.9980	3.20–800.00	3.20 ± 0.25	3.23
Atractylenolide I	$y = 0.02736x + 0.04174$	0.02736 ± 0.00097	0.04174 ± 0.13011	0.9963	1.52–380.00	1.52 ± 0.21	6.12
Glycyrrhetinic acid	$y = 0.00479x + 0.13598$	0.00479 ± 0.00031	0.13598 ± 0.11530	0.9958	3.44–860.00	3.44 ± 0.45	8.12

Abbreviation: SE, standard error.

established calibration curve to determine the corresponding plasma drug concentrations. These concentration–time data were subsequently analyzed using DAS pharmacokinetic software (version 3.2.8). The resulting concentration–time profiles are presented in Figure 7 and the derived pharmacokinetic parameters are summarized in Table 3. Pharmacokinetic analysis revealed the rapid absorption of liquiritin (as indicated by its early T_{max}), a short half-life, and brief in vivo residence time, which were consistent with its metabolic profile. Although the levels of ligustilide were the highest in vitro, it did not achieve the highest AUC. Its rapid absorption (based on T_{max}) suggested extensive metabolism to be likely responsible for its relatively low systemic exposure. In contrast, compounds such as costunolide, atractylenolide I, and dehydrocostus lactone exhibited slower absorption and elimination kinetics, prolonging their systemic retention. Glycyrrhetinic acid exhibited comparatively slow absorption and elimination rates, leading to extended systemic circulation and prolonged exposure to increased concentrations. It had the largest area under the curve $(AUC)_{0\text{-}t}$ and $AUC_{0\text{–}\infty}$ values, potentially attributable to the efficient in vivo metabolic conversion of glycyrrhizic acid—abundantly present in *Glycyrrhiza* in GPP—into glycyrrhetinic acid.

4 | Discussion

This study is the first of its kind to systematically elucidate the association between the in vivo metabolic network of multiple components in GPP and their pharmacokinetic behaviors. At the metabolic level, six major classes of components exhibited specific transformation patterns. Phenylpropanoids (e.g., coumarin N72) were primarily metabolized via Phase I reactions, including hydration (MA1), ketone reduction (MA2), aromatic

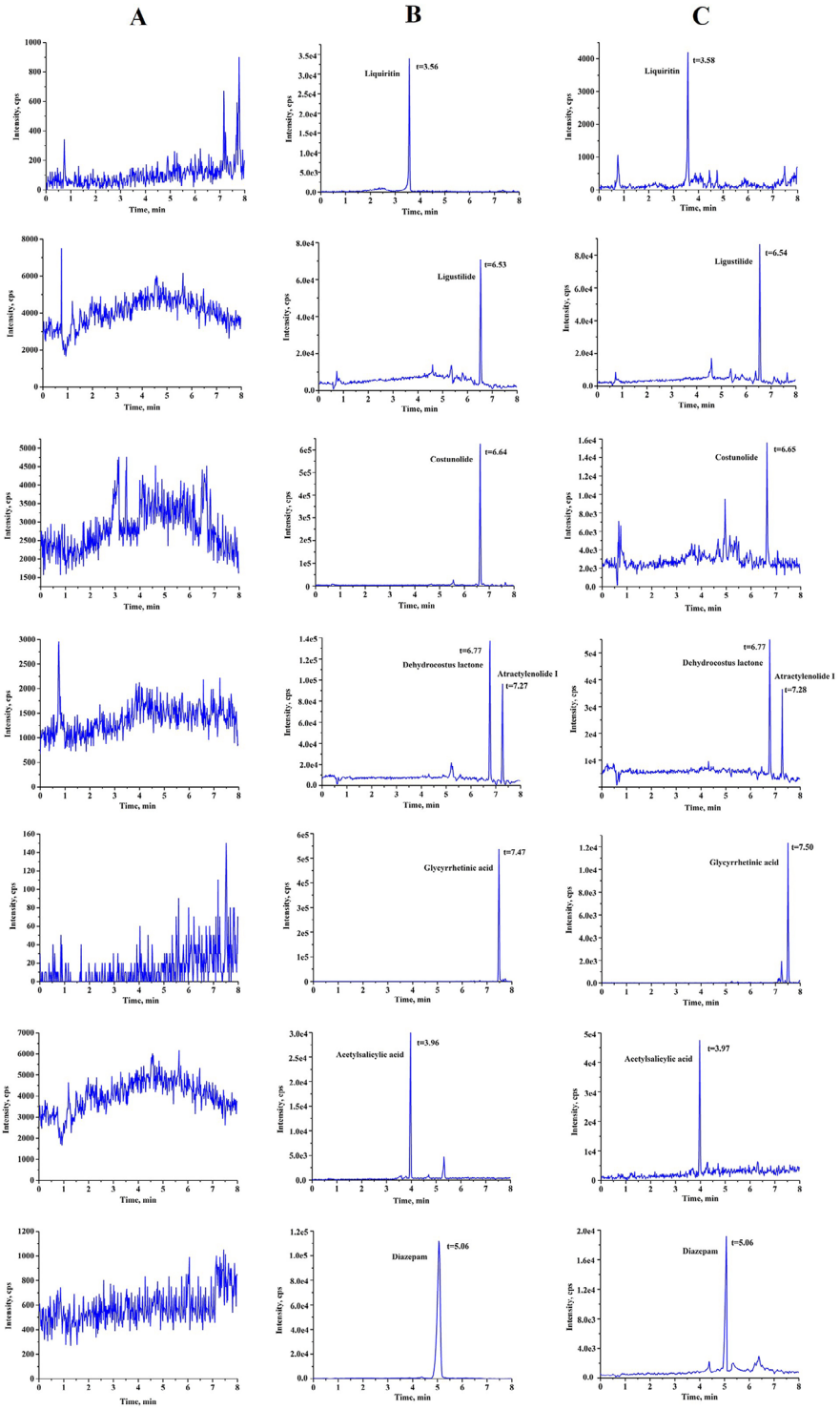

FIGURE 7 | Mean plasma concentration-time curves of six analytes after oral administration of GPP in rats (mean ± SD, $n = 6$).

ring oxidation (MA3), and methylation (MA4) reactions to generate four metabolites, with its ring-opening/reduction reactions potentially mitigating hepatotoxicity [25]. Flavonoids and their glycosides followed a core pathway of "deglycosylation-secondary modification," where liquiritin–isoliquiritin were hydrolyzed to aglycones (liquiritigenin MB2/isoliquiritigenin MB5) followed by A/B ring-specific oxidation (MB3/MB4), glucuronidation (MB6/MB9), and sulfation (MB1), suggesting a "deglycosylation–activation/conjugation–detoxification" pattern underlying their biphasic regulatory effects. Terpenoids and their glycosides, as major bioactive constituents, exhibited highly complex metabolism—triterpenoid saponins (polygalasaponin N63, astragaloside IV N69) adhered to the "sugar chain hydrolysis → aglycone modification" route, with the polygalasaponin hydrolyzate (MC1) forming oxidized (MC2) or double bond-reduced (MC3) products and astragaloside IV hydrolysis yielding cycloastragenol (MC4), which was subsequently sulfated to MC5, indicating that sulfation may prolong its systemic residence.

TABLE 3 | The pharmacokinetic parameters for six analytes in vivo after gavage with Guipi Pill ($n = 6$, mean ± SD).

Analyte	AUC_{0-t} (μg/L·h)	$AUC_{0-\infty}$ (μg/L·h)	$t_{1/2}$ (h)	T_{max} (h)	C_{max} (μg/L)	MRT_{0-t} (h)	$MRT_{0-\infty}$ (h)	CLz/F (L/h/kg)
Liquiritin	918.44 ± 74.63	920.72 ± 72.96	2.82 ± 0.73	0.36 ± 0.06	383.35 ± 30.23	4.02 ± 0.51	4.59 ± 0.69	0.21 ± 0.02
Ligustilide	762.70 ± 355.01	789.34 ± 369.61	8.42 ± 3.09	0.25 ± 0.14	167.81 ± 62.30	9.04 ± 3.97	11.23 ± 4.15	4.35 ± 1.85
Costunolide	601.59 ± 210.20	651.62 ± 226.31	15.17 ± 3.16	2.50 ± 1.23	54.42 ± 9.48	12.11 ± 2.31	16.85 ± 2.20	1.01 ± 0.34
Dehydrocostus lactone	1121.13 ± 140.06	1256.96 ± 178.81	12.56 ± 2.15	5.67 ± 0.82	81.01 ± 8.97	15.23 ± 1.28	20.80 ± 2.18	0.98 ± 0.13
Atractylenolide I	682.02 ± 217.10	724.98 ± 225.61	2.19 ± 0.10	1.33 ± 0.52	82.40 ± 13.74	10.32 ± 1.30	14.51 ± 2.46	0.02 ± 0.004
Glycyrrhetinic acid	10550.67 ± 1334.58	11255.58 ± 1427.82	11.08 ± 2.91	8.33 ± 0.82	712.55 ± 59.21	14.84 ± 0.90	16.74 ± 1.41	0.03 ± 0.002

Sesquiterpene lactones (atractylenolide III N86, atractylenolide I N99) underwent unique reactions such as reduction (MC11), heterocyclic cleavage-reduction (MC25), and decarboxylation (MC26), with lactone ring alterations potentially impacting their anti-inflammatory effects [26–28]. Volatile oils (e.g., ligustilide H N41) and organic acids (e.g., ferulic acid N32) were predominantly metabolized via Phase II conjugation reactions, undergoing sulfation (MD1/ME2) and glycine conjugation (ME1) reactions, respectively, to enhance water solubility and accelerate excretion. Polyacetylenic glycosides (lobetyolin) were hydrolyzed to form a novel compound (MF1), which further underwent ω-oxidation (MF3), alcohol oxidation (MF4), and reduction (MF2), suggesting oxidative metabolism of its terminal alkyne bond to likely contribute to immunomodulatory activity [29].

Pharmacokinetic metabolism correlation analysis revealed the following key mechanisms: Liquiritin was rapidly absorbed (early T_{max}) but exhibited a short half-life (small $t_{1/2}$) and limited exposure (AUC) due to extensive deglycosylation and Phase II conjugation reactions. The high ligustilide content (1158.32 μg/g) in the formulation contrasted with its low AUC and was attributable to significant first-pass metabolism (e.g., oxidative sulfation MD3) following its rapid absorption, indicating an oral bioavailability bottleneck. Sesquiterpene lactones (e.g., costunolide and atractylenolide I) achieved sustained systemic exposure due to slow absorption and elimination (long $T_{max}/t_{1/2}$), with their metabolic inertness (e.g., atractylenolide I requiring multistep transformation) potentially underpinning long-lasting effects. Glycyrrhetinic acid exhibited outstanding pharmacokinetic characteristics, achieving the highest $AUC_{0-\infty}$ likely derived from the efficient hydrolytic conversion of glycyrrhizic acid in the formula, while its slow elimination (long MRT) led to sustained plasma concentration, aligning remarkably with the "slow-tonifying" efficacy profile of GPP [30].

Overall, our findings indicate that GPP achieves synergistic efficacy through its "multicomponent metabolic complementarity": flavonoid glycosides can provide their rapid effects via quick release, terpenoid components sustain the long-term action of the preparation via their slow-release metabolism, and glycyrrhetinic acid acts as a metabolic hub that integrates overall systemic exposure. The multidimensional "component-metabolism-pharmacokinetic" relationship elucidated in this study could serve as a novel paradigm to elucidate the holistic mechanisms of action of several other complex traditional medicinal formulae.

5 | Conclusions

UHPLC-Q-Exactive Orbitrap MS technology was used to analyze the plasma, bile, urine, and fecal samples of rats administered GPP via oral gavage. A total of 106 compounds derived from six major structural classes, comprising 48 prototypes and 58 metabolites, were identified, which included nine potentially novel compounds. The metabolic pathways that were identified included methylation, double bond reduction, hydroxylation, heterocyclic ring cleavage, sulfation, and glucuronidation. Concurrently, pharmacokinetic studies on the six prototype compounds from different structural classes were conducted using UHPLC-MS/MS, and the pharmacokinetic parameters were determined

to be consistent with their structural characteristics. This study provides the preliminary elucidation of the in vivo metabolic and pharmacokinetic profiles of the principal components of GPP, thereby establishing a strong foundation for research into its pharmacodynamic material basis, facilitating further mechanistic investigations of its active constituents, and supporting its rational clinical applications.

However, our study has some limitations. Although multiple metabolic pathways were identified, the specific metabolic enzymes mediating these reactions have not been ascertained. Additionally, the pharmacokinetic studies failed to cover all critical prototype components and important active metabolites. Future studies could utilize liver microsomes, recombinant enzymes, and other tools to identify the specific isoforms of the metabolic enzymes responsible for the key metabolic steps of the main components of GPP and elucidate their enzyme kinetic characteristics. Furthermore, pharmacokinetic research should be extended to encompass more significant prototype components and key metabolites confirmed to be active, thereby comprehensively delineating the complex in vivo exposure profile of GPP.

Author Contributions

The authors acknowledge the editors and reviewers for their time and effort in handling this manuscript.

Acknowledgment

This work was supported by a rolling funding project for Liaoning distinguished professors (2017), and the Science Research Fund Project of Liaoning Provincial Department of Education (Grant Number. JYTMS20231404).

Conflicts of Interest

The authors declare no conflicts of interest.

References

1. Y. D. Li, E. P. Xu, L. J. Kang, N. N. Ding, X. J. Yang, and E. H. Zhou, "Research Progress of Guipi Decoction and Combined Formula in Treating Depression," *Chinese Archives of Traditional Chinese Medicine* 41 (2023): 148–154.

2. X. B. Ye, "Research Progress in Pharmacological Action and Clinical Application of Guipi Pill," *Guangming Journal of Chinese Medicine* 36 (2021): 493–496.

3. X. Y. Yu, H. Q. Xu, L. Liu, and S. B. Sun, "Effect of Gui-pi Decoction on Learning Memory and Hippocampal Morphology in Mice Exposed to Benzene," *Journal of Environmental & Occupational Medicine* 28 (2011): 149–155.

4. P. Xu, J. Q. Jia, E. J. Jiang, L. P. Kang, and K. L. Wu, "Protective Effect of an Extract of Guipi Pill Against Radiation-Induced Damage in Mice," *Chinese Journal of Integrative Medicine* 18 (2012): 490–495.

5. L. Liu, S. F. Wang, R. Xu, and X. M. Peng, "Effects of Guipi Pill on Bone Marrow Cell Cycle of Mice Exposed to Benzene," *Chinese Journal of Integrated Traditional and Western Medicine* 33 (2013): 380–384.

6. Y. J. Liu, L. Liu, and J. Wang, "Effects of Inspissated Guipi Pill on T Cell Sunsets, Serumal Hemolysin and Granulocyte Colony Stimulating Factor of Benzene Poisoning Mice," *China Journal of Traditional Chinese Medicine and Pharmacy* 31 (2016): 5256–5259.

7. S. X. Li, G. X. Yuan, Y. Ma, and Y. T. Wang, "Study on Immunomodulatory Effect of Guipi Pills on D-Galactose-Induced Aging Mice," *China Pharmacy* 34 (2023): 1426–1430.

8. H. F. Bai, F. X. Qin, T. Zhen, N. N. Yuan, and L. X. Sun, "Mechanism of Guipi Pills in Treatment of Anxiety Disorder Based on UHPLC-Q-Exactive Orbitrap MS and Network Pharmacology," *Chinese Journal of Modern Drug Application* 40 (2023): 25–37.

9. Y. Q. Liu, Y. L. Li, R. Zhang, M. Y. Qin, Y. L. Xi, and Q. H. Li, "Research Progress on Anti-Depression Mechanism of Spleen-Wan Powder and Its Active Components," *Traditional Chinese Medicine* 12 (2023): 806–813.

10. Y. Liu, G. R. Han, and S. H. Feng, "Assay of Glycyrrhizic Acid and Ligustilide in Guipi Pill by HPLC," *Chinese Traditional Patent Medicine* 34 (2012): 667–669.

11. J. J. Deng and L. E. Sun, "Determination of Costunolide and Dehydrocostuslactone in Guipi Pills by HPLC," *Strait Pharmaceutical Journal* 26 (2014): 76–78.

12. H. K. Cai, X. F. Liu, F. R. Jiang, H. L. Gao, Y. H. Xia, and G. X. Sun, "RP-HPLC Determination of Liquiritin, Ferulic Acid, Ammonium Glycyrrhetate and Dehydrocostus Lactone in Guipi Pills 12(Concentrated Pills)," *Central South Pharmacy* 12 (2014): 1242–1245.

13. L. C. Bai, P. Y. Chen, J. Q. Xu, T. T. Wang, H. Han, and P. L. Dong, "Comprehensive Profiling of Chemical Constituents and Metabolites of the *Angelica Sinensis–Sophora Flavescens* Herbal Pair in Plasma and Urine via UHPLC-Q-TOF-MS Coupled with Multi-Platform Data Integration," *Journal of Separation Science* 48 (2025): e70201.

14. M. L. Wang, H. R. Li, C. M. Liu, Y. Y. Zhang, Q. Wu, and Y. B. Yang, "Lingguizhugan Decoction Improved Obesity by Modulating the Gut Microbiota and Its Metabolites in Mice," *Current Drug Metabolism* 25 (2024): 276–287.

15. J. Chen, J. Li, F. Wang, R. R. Ge, L. Wang, and J. L. Huang, "Metabolite Profiling of Liquiritin in Acute Myocardial Infarction Model Rat After Intragastric Administration Using an Information-Dependent Acquisition-Mediated Ultra-High-Performance Liquid Chromatography-Tandem Mass Spectrometry Method," *Biomedical Chromatography* 38 (2024): 1–9.

16. S. Jiang, S. P. Wang, P. P. Dong, X. Wei, P. Gao, and J. Y. Zhang, "A Comprehensive Profiling and Identification of Liquiritin Metabolites in Rats Using Ultra-High-Performance Liquid Chromatography Coupled With Linear Ion Trap–Orbitrap Mass Spectrometer," *Xenobiotica* 51 (2021): 564–581.

17. Z. P. Zhu, J. Wang, L. H. Huang, and T. H. Gao, "Research on Chemical Constituents and Metabolic Processes of Yuanzhi Saponin," *Pharmacy and Clinics of Chinese Materia Medica* 7 (2016): 61–65.

18. S. L. Yuan, J. Q. Chen, Y. W. Cao, et al., "Investigation of Bioactive Components and Metabolic Pathways of Zhen-Wu-Tang in Rat Plasma and Renal Tissue by UHPLC-Q-TOF/MS," *Phytochemical Analysis* 36 (2024): 1–22.

19. L. Wang, F. Xv, G. X. Liu, M. Y. Shang, and S. Q. Cai, "Analysis of the Metabolites of Ethyl Acetate Extract From *Angelica sinensis* in Rats by HPLC-MS^n," *China Pharmacy* 25 (2014): 4425–4430.

20. S. M. Tao, H. D. Li, and J. Liu, "Metabolic Profiling of Ligustilide and Identification of the Metabolite in Rat and Human Hepatocytes by Liquid Chromatography Combined with High-Resolution Mass Spectrometry," *Journal of Separation Science* 43 (2020): 4405–4413.

21. W. Zhang, S. Jiang, D. W. Qian, H. L. Guan, H. Ren, and J. A. Duan, "Study on Metabolism of Ferulic Acid Produced by Intestinal Bacteria," *Chinese Journal of Analytical Chemistry* 2 (2014): 244–248.

22. X. B. Qin, J. H. Wang, L. L. Yu, et al., "Rapid Identification of Chemical Constituents in Qubai Babuqi Tablets by Ultra-High-Performance Liquid Chromatography Quadrupole-Orbitrap-Mass Spectrometry," *Journal of Separation Science* 48 (2025): e70117.

23. L. Liu, J. A. Duan, Y. P. Tang, D. W. Qian, S. L. Su, and P. Liu, "Study on Metabolites of Taohong Siwu Tang in Dysmenorrhea Model Rats," *Pharmacology and Clinics of Chinese Materia Medica* 31 (2015): 1–4.

24. H. F. Bai, T. Zhen, H. J. Wang, H. Y. Li, and L. X. Sun, "Simultaneous Determination of Fourteen Constituents in Guipi Pills by UHPLC-ESI-MS/MS," *Chinese Traditional Patent Medicine* 45 (2023): 2138–2144.

25. M. Pitaro, N. Croce, V. Gallo, A. Arienzo, G. Salvatore, and G. Antonini, "Coumarin-Induced Hepatotoxicity: A Narrative Review," *Molecules* 27 (2022): 1–19.

26. Y. Zhou, S. H. Huang, F. L. Wu, et al., "Atractylenolide III Reduces Depressive- and Anxiogenic-Like Behaviors in Rat Depression Models," *Neuroscience Letter* 759 (2021): 1–7.

27. A. Paco, T. Bras, J. O. Santos, P. Sampaio, A. C. Gomes, and M. F. Duarte, "Anti-Inflammatory and Immunoregulatory Action of Sesquiterpene Lactones," *Molecules* 27 (2022): 1–22.

28. W. Kuang, Y. Wang, Y. X. Huang, W. L. Wu, and M. Zhang, "Rapid Identification of the Compounds of Bushen Huoxue Prescription Based on Offline Two-Dimensional Liquid Chromatography With High-Resolution Mass Spectrometry and Molecular Network Technology," *Journal of Separation Science* 47 (2024): e2300624.

29. Q. Xie, H. X. Wang, H. D. Guan, et al., "The in Vitro/in Vivo Metabolic Pathways Analysis of Lobetyol, Lobetyolin, and Lobetyolinin, Three Polyacetylenes From Codonopsis Radix, by UHPLC-Q/TOF-MS and UHPLC-MS/MS," *Journal Of Pharmaceutical And Biomedical Analysis* 223 (2023): 1–13.

30. T. Suzuki, M. Tsukahara, Y. Akasaka, and H. Inoue, "A Highly Sensitive LC-MS/MS Method for Simultaneous Determination of Glycyrrhizin and Its Active Metabolite Glycyrrhetinic Acid: Application to a Human Pharmacokinetic Study After Oral Administration," *Biomedical Chromatography* 31 (2017): e4032.

Supporting Information

Additional supporting information can be found online in the Supporting Information section.

Supporting Information file 1: jssc70257-sup-0001-SuppMat.docx.